Large-Deformation Behavior of Honeycomb-Structured Polymer Sheets as a Function of Polar Angle

Kwang-Yong Jin, Dae-Yoon Kim, So-Eun Kim, Shiao-Wei Kuo, Joong Hee Lee, Min-Young Lyu, Seok-Ho Hwang, Alan N. Gent, Changwoon Nah,* Kwang-Un Jeong*

To construct the structure/property relationships of patterned polymer architectures depending on symmetry, the large-deformation behavior of 2D HSPS with respect to the polar angle was studied. Holes aligned along the HSPS apex were more effective in decreasing tensile force and reducing stress concentration than those located along the plane. On varying the polar angle from 0 to 30°, the tensile force fluctuated up and down like an undamped negative sinusoidal wave with a wavelength of 15°. Additionally, molecular orientations of HSPS were monitored in situ. By comparing experimental measurements with computer simulations, it was concluded that the tensile force depends on the number of holes as well as the orientation of the axes of the honeycomb structure.

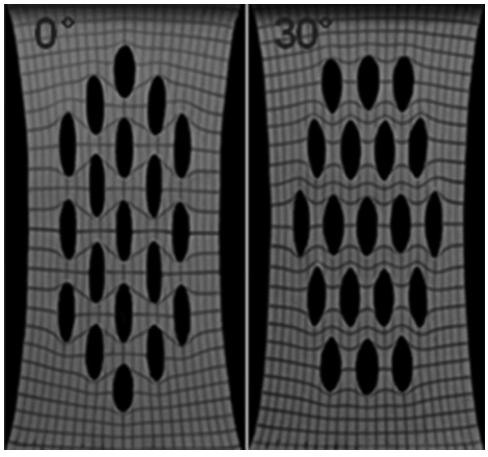

K.-Y. Jin, D.-Y. Kim, S.-E. Kim, J. H. Lee, C. Nah, K.-U. Jeong
Department of Polymer-Nano Science and Technology, and Polymer Materials Fusion Research Center, Department of BIN Fusion Technology, Chonbuk National University, Jeonju, Jeonbuk 561-756, Korea
E-mail: kujeong@jbnu.ac.kr, cnah@jbnu.ac.kr
S.-W. Kuo
Department of Materials Science and Optoelectronic Engineering, National Sun Yat-Sen University, Kaohsiung 804, Taiwan
M.-Y. Lyu
Department of Die and Mould Design, Seoul National University of Technology, Seoul, 139-743, Korea
S.-H. Hwang
Department of Polymer Science and Engineering, Dankook University, Yongin 448-701, Korea
A. N. Gent
College of Polymer Science and Polymer Engineering, The University of Akron, Akron, OH 44325-3909, USA

Introduction

Even though many mechanical properties of polymers, including elastic modulus, toughness, and strength, have been intensively studied, the deformation behaviors of the patterned polymeric materials especially under the large deformations remain as significant scientific challenges.[1] The mechanical deformation of the periodically patterned polymer structure is of scientific interest and also relevant in practical applications,[2–8] such as in smart membranes,[9] in tunable photonic/phononic crystals,[10] in adjustable microlens and in porous templates for cell culture.[11–16]

Up to now, the patterned structures from one (1D) to three dimensions (3D) can be fabricated in the different length scales[17–19] by supramolecular chemistry,[20,21] self-assembly of block copolymers (BCP),[22,23] breath figure (BF)

DOI: 10.1002/macp.201000708

method,[24] and lithographic techniques.[25] Of these fabrication methods, the self-assembly of BCP is a promising way to achieve the periodic pattern in the range of 10 to 100 nm,[26] which depends on the molecular structure, molecular weight and volume ratio of each block. BF seems to be the most promising method to fabricate 2D periodic patterns in the size range from 50 nm to 20 μm. Solution casting under a high humidity can lead to the periodic structures consisting of spheres, columns, or lamellae.[27–29] Although the self-assembly techniques can provide rapid routes to form the periodically patterned structures from nanometer to micrometer length scales, it is extremely difficult to avoid the formation of defects without any external forces and confinements.[30] An alternative fabrication method to minimize defects during fabrication is the lithographic technique (top-down method). However, the lithographic techniques are complicated and tedious compared to self-assembly (bottom-up method).[31] Recently, there have been many attempts to fabricate defect-free patterned structures by combining top-down and bottom-up methods.

Owing to their unique deformation properties and potential applications, the mechanical deformations of the periodically patterned structures at different dimensions and length scales have attracted a lot of scientists and engineers.[32] The mechanical deformations of the self-assembled BCP were studied by small-angle X-ray scattering (SAXS) and transmission electron microscopy (TEM) combined with cross-polarized optical microscopy (POM).[33,34] Using the elastic compliance tensor, the small deformation behaviors of the patterned BCPs were explained. Furthermore, SAXS results provided the microscopic information on the evolution of the microdomain morphology.[35,36] However, there were limitations at the large deformations in describing the deformation of microstructures even though they recognized several important features at the small deformations. Utilizing TEM combined with SAXS, the large deformation behaviors of BCP thermoplastic elastomers were also studied.[37,38] From this, it was concluded that kinking and faulting was observed during mechanical deformations.

The investigation of the mechanical deformation of the patterned polymeric materials is hindered because of the existence of defects. Furthermore, the correlation between the mechanical property and the deformed morphology is quite limited since it is difficult to match the deformation direction to the symmetrical axes of the patterned structures. In this research, alternative ways were used for investigating the large deformations. 2D honeycomb-structured polymer sheets (HSPS) were prepared in an acrylonitrile butadiene rubber (NBR) which can be deformed more than 300% elongation without breaking. The honeycomb features had a length scale in the range of millimeters. The honeycomb structure was chosen in this research because of the high interests in its potential applications in electronics, photonics, biotechnology, and material technology. Simple tensile tests were conducted with respect to the deformation directions and the number of holes, and their results were compared with those of finite element analysis (FEA). Additionally, the molecular orientations at different locations were investigated using cross-polarized films. It was concluded that the tensile forces at the large deformations depend not only on the number of holes but also on the relative orientation of the honeycomb structure. The structure/property relationships of HSPS can be applied to the design of patterned polymer architectures with specific properties.

Experimental Part

Materials

NBR (Kumho Petroleum Chemical Co., Korea) that can be deformed more than 300% elongation without a catastrophic failure was used to fabricate the HSPS. The chosen NBR contained 34 wt.-% acrylonitrile and its Mooney viscosity was 41 (ML_{1+4} at 100 °C). ZnO (Hanil Co., Korea) and stearic acid (S/A) (Pyungwha Co., Korea) were also applied as vulcanization activators. Additionally, *tert*-butyl-2-benzothiazylsulfenamide (TBBS, Bayer Co., Belgium) and sulfur (Seikwang Co., Korea) were added as vulcanization accelerator and curing agent, respectively.[39] The compound formulation typically used in the industry (ASTM D3182 and D3184) was chosen. A transparent polydimethylsiloxane (PDMS, Dow Corning, Sylgard 184) prepared by thermal crosslinking was selected as the material instead of NBR for the observation of birefringence under cross-polarized films. After degassing the PDMS mixture (with 10 wt.-% crosslinker) for 1 h, the mixture was thermally crosslinked at 65 °C for 12 h.

Sample Preparation

The formulated NBR was prepared by mixing ingredients in the ratio of NBR = 100 phr, ZnO = 5 phr, S/A = 1 phr, TBBS = 1 phr and S = 2 phr.[39] The formulated NBR was homogeneously mixed for 15 min using a two-roll mill (Mixing roll M/C DS-1500R, roll diameter = 12 in) at 15.3 rpm. The NBR mixture was further dried at ambient condition for 1 h. Utilizing an oscillation disk rheometer (ODR-2000, Alpha technology), the optimized vulcanization time was estimated to be 20.6 min. Under the optimized vulcanization conditions, NBR sheets were fabricated using a compression press device (CMV50H-15-CLPX, CARVER). The thicknesses of NBR sheets were controlled to be in the range of 0.5 to 2 mm by applying metal spacers between two compression plates. NBR sheets with a uniform thickness to within 0.01 mm were prepared with dimensions of $72 \times 92 \times 1\ mm^3$, as illustrated in Figure 1b.

As shown in Figure 1a, the dumbbell-shaped specimen was also prepared according to the procedure described in ASTM D412 to evaluate the edge effects of rectangular-shaped samples. In the rectangular-shaped samples, the shaded areas ($72 \times 10\ mm^2$) were the sample holding areas during the tensile test. To describe the

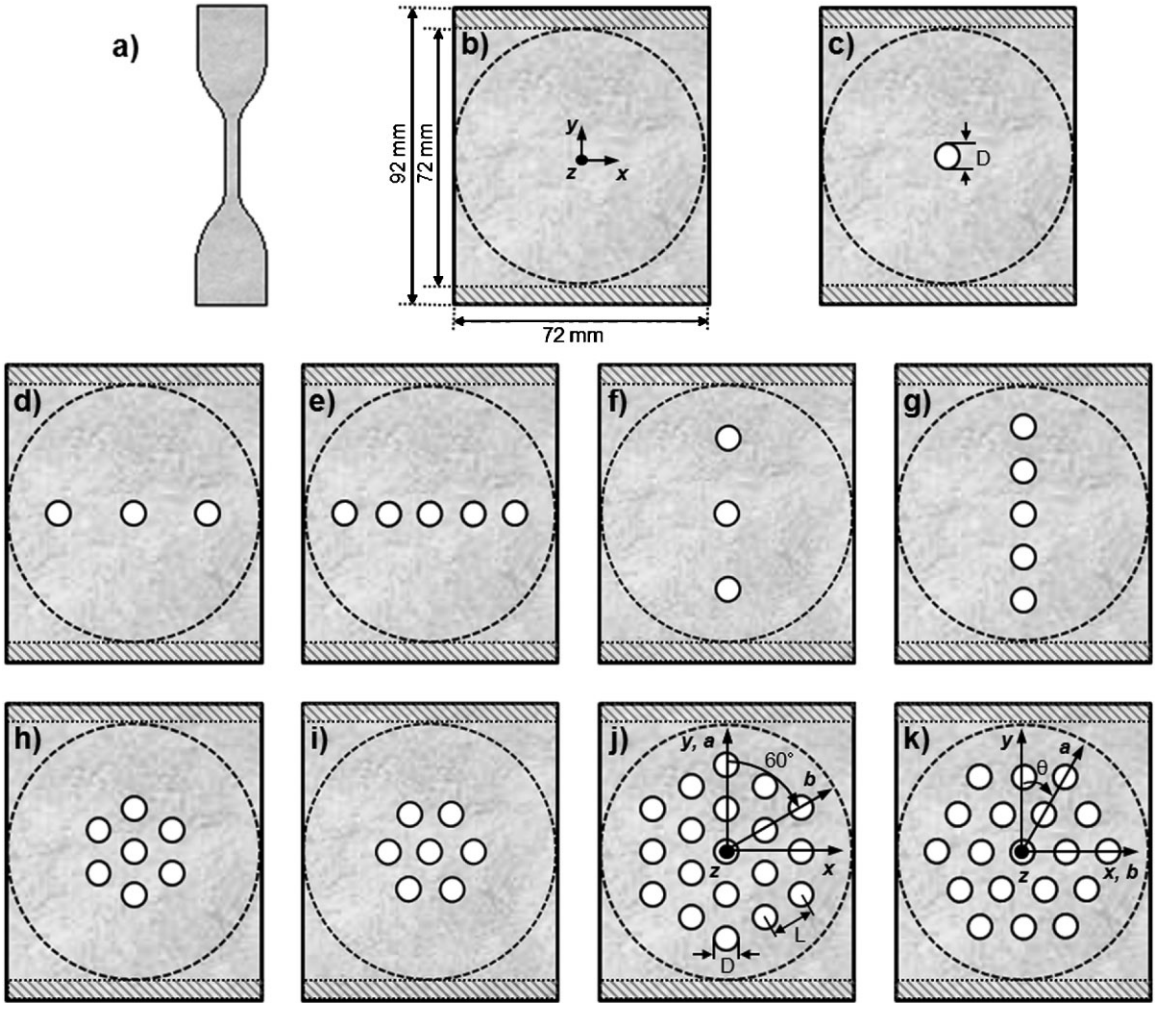

Figure 1. Schematic illustration of specimens: (a) ASTM D412 dumbbell-shaped specimen and rectangular specimen (b) without holes, (c) with 1 hole, (d, f) with 3 holes, (e, g) with 5 holes, (h, i) with 7 holes, and (j, k) with 19 holes. Figure 1d and f have three holes on the transverse direction (*x*-axis) of HSPS with 0° polar angle (Figure 1j) and on the machinery direction (*y*-axis) of HSPS with 30° polar angle (Figure 1k), respectively. Figure 1e and g have five holes on the transverse direction (*x*-axis) of HSPS with 30° polar angle (Figure 1k) and on the machinery direction (*y*-axis) of HSPS with 0° polar angle (Figure 1j), respectively. Figure 1h and i are HSPS with seven holes corresponding to Figure 1j (0° polar angle) and 2k (30° polar angle), respectively.

sample geometry and the honeycomb structure, two different Cartesian coordinators were applied in this study. One was for the rectangular-shaped sample (*x, y, z*) and the other was for the 2D honeycomb structure (*a, b*). The *x*-axis and *y*-axis were the transverse and machinery directions, respectively, while the *z*-axis stands for the sample thickness. The rectangular samples were stretched along the *y*-axis (machinery direction) so that the stretched length variation of *y*-axis indicates the elongation of sample. Because the structure in the rectangular sample was the 2D honeycomb structure, the *a*-axis was identical to the *b*-axis and *r*-angle was 60°. As illustrated in Figure 1j, the polar angle was defined as the angle between *y*-axis (machinery direction) and *a*-axis. When the polar angle was 0° (Figure 1j), the machinery direction (*y*-axis) was parallel to the apex of honeycomb structure (*a*-axis), while the polar angle = 0° means that the machinery direction was parallel to the face of honeycomb structure ([11]-direction). Note that the *xyz* Cartesian coordinate does not change even though the honeycomb structure was rotated from 0 (Figure 1j) to 30° (Figure 1k). The 2D HSPS consisted of 19 holes with a diameter (*D*) of 6 mm. The distance (*L*) between the centers of neighboring 6 holes was 12 mm, as illustrated in Figure 1j. To study the effect of mechanical properties depending on the number of holes, the rectangular samples with holes from 1 to 7 were also prepared, as shown in Figure 1c–i. Circular holes in the 2D HSPS were created by a compression puncher. Special attention should be paid to minimize the creation of defects during the punching process. Additionally, square meshes with a unit cell dimension of $3 \times 3\ mm^2$ were drawn on the in-plane (*xy*-plane) surface of the rectangular samples for the in situ investigation of local deformations and stress concentrations during mechanical deformation.

Moreover, to identify the molecular orientations at specific locations during the mechanical deformation, the birefringence of PDMS HSPS was monitored with respect to the polar angle.

Mechanical Deformations of HSPS

Utilizing a tensile tester equipped with an extensometer (Long Travel Extensometer, LLOYD Instruments) with a 5 kN load cell, tensile tests were performed at a cross-head speed of 50 mm s^{-1}. To secure the sample holding, laboratory-designed T-shaped grips were used to stretch the rectangular specimens. The molecular orientations at specific locations of the PDMS HSPS were monitored. Here, the polarizing axes were aligned to be parallel and perpendicular to the machinery direction. A white backlight was irradiated through the cross-polarized films and the PDMS HSPS, and the birefringence was recorded using a digital camera (COOLPIX S6, Nikon). Note that since the mechanical failure of the PDMS HSPS occurs above the 25% elongation, the tensile stress of the PDMS HSPS was obtained at the 20% elongation and its result was compared with that of NBR HSPS at 80% elongation. Since the mechanical deformation above 10% elongation was considered as a large deformation,[1] this comparison should be acceptable and the results were did not differ much.

Computer Simulation

FEA computer simulation was performed based on the experimental properties of NBR (Young's Modulus = 11.6 MPa, Poisson ratio = 0.4993) utilizing Abaqus version 6.7. 3D shell elements with four-node bilinear plain strain was applied for the calculation. The total numbers of elements were in the range of 9 000–9 200.

Results and Discussion

Tensile Properties of Rectangular Specimen as a Function of the Number of Holes

Before investigating the mechanical deformation behavior of 2D HSPS, the intrinsic mechanical properties of the NBR matrix are evaluated by a tensile tester. Both tensile forces and stresses of the dumbbell-shaped specimen (ASTM D412,[40,41] Figure 1a) and the rectangular specimen without any holes (Figure 1b) are represented in Figure 2. As expected, the tensile force of the rectangular specimen without any hole is higher in all strain regions than that of the dumbbell-shaped specimen, while its ultimate tensile strain is lower than that of the dumbbell-shaped specimen. This result should originate from the local stress concentrations as well as the geometric differences and the edge effects of the rectangular specimen. This explanation can be further supported by the fact that the tensile stress of the rectangular specimen is higher than that of the dumbbell-shaped specimen. The purpose of this research is to evaluate and understand the mechanical deformation properties of

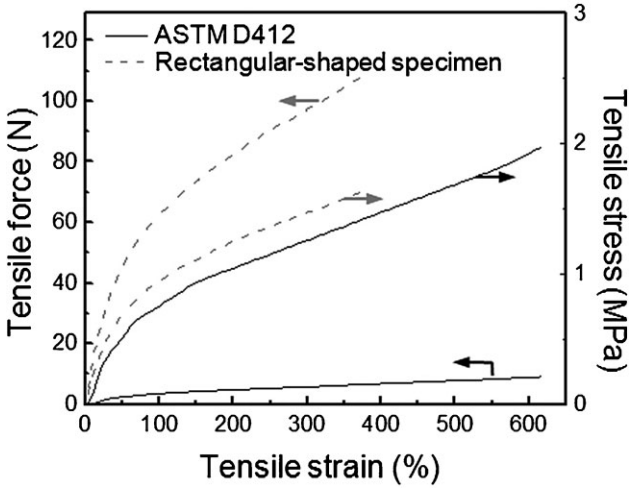

Figure 2. Tensile force and stress with respect to tensile strain of ASTM D412 dumbbell-shaped specimen and rectangular specimen without any hole.

the 2D HSPS containing artificial defects (holes) arranged in a honeycomb symmetry. In this system, it is complicate to use the tensile stress, since the cross-sectional area of 2D HSPS is changed with the polar angles and the number of holes. Therefore, the tensile force will be used in the following discussion rather than the tensile stress and its value is compared with that of the rectangular specimen without any hole.

To construct the structure/property relationships of the patterned polymer architecture depending on the symmetry, the mechanical properties of the rectangular specimens with different numbers of holes (n) are first investigated. The tensile forces with respect to the strains of the rectangular specimen (schematically illustrated in Figure 1) with holes from 0 to 19 are shown in Figure 3a and their tensile forces at the 80% elongation are also summarized in Figure 3b. It is realized that Young's modulus of the rectangular specimen does not depend on the number of holes. This result confirms that the structural defects do not much affect the mechanical properties at small deformations. However, by increasing the number of holes in the rectangular specimen, the tensile forces at 80% elongation (a large deformation) decrease exponentially from 57.4 ($n = 0$) to 48 MPa ($n = 7$) and gradually level down to 46 MPa ($n = 19$), as shown in Figure 3b. Here, we have to emphasize the experimental observation that the holes arranged along the machinery direction (y-axis on Figure 1f and g) are more effective to decrease the tensile forces than the holes punched perpendicular to the machinery direction (parallel to the transverse direction, x-axis). This result can be explained by the edge effect. When the holes are arranged along the transverse direction (Figure 1d and e), the stresses are mainly concentrated on the transverse direction, which leads to a higher edge effect than the cases

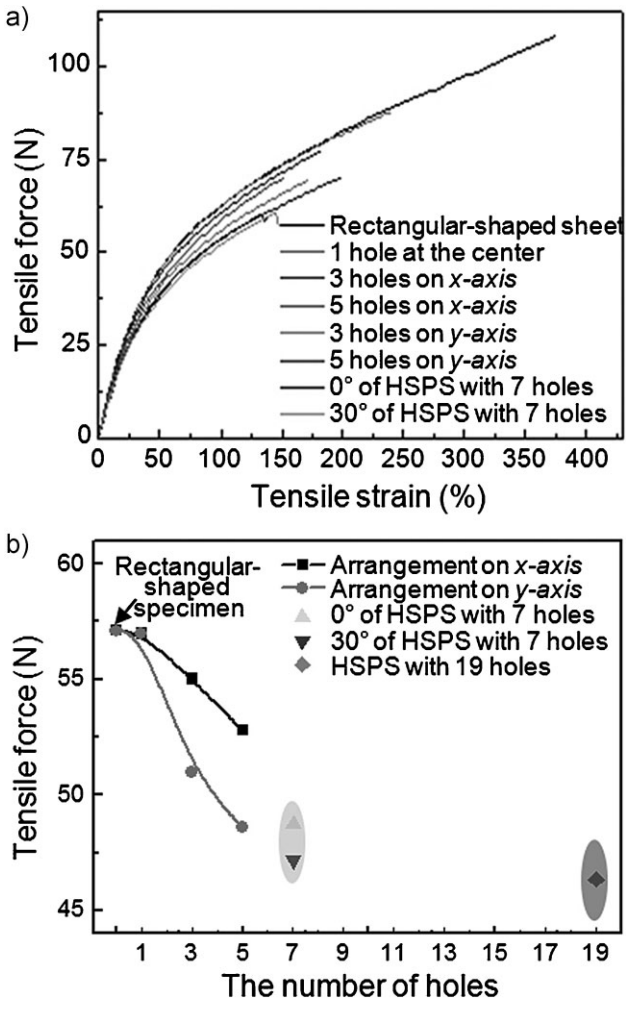

Figure 3. (a) Tensile force/strain curve of rectangular specimen for 0 to 19 holes, and (b) tensile force of rectangular specimen as a function of the number of holes from 0 to 19 holes.

(Figure 1f and g) of holes punched along the machinery direction. This means that the higher tensile force is needed to push the sample along the transverse direction for the sample with holes along the transverse direction. Another plausible explanation can be found from the cooperative deformation of holes, which will be discussed in Figure 4.

Stress concentration and distribution on the rectangular specimen with $n = 1$ to $n = 7$ holes are monitored and the photographs of the rectangular specimen at 80% elongation are shown in Figure 4a–g, respectively. Before the mechanical deformation, the square meshes with a unit cell dimension of $3 \times 3\ mm^2$ are additionally drawn on the in-plane (*xy*-plane) surface of the rectangular samples for the in situ investigations of the local deformations and the stress concentrations. When the rectangular specimens with the holes along the transverse direction are elongated, the circular holes are stretched along the machinery direction and simultaneously squeezed along the transverse direction, as shown in Figure 4b and c. By increasing the number of holes along the transverse direction, the tensile forces at 80% elongation decrease, as already discussed in Figure 3, and the aspect ratios of the deformed holes decrease as moving out of the center. Therefore, the stress is concentrated most at the side edge of the central holes (Figure 4b and c) and only the central holes keep the C_{2v} symmetry and the last of them show the C_2 symmetry due to the asymmetrically elongated conditions. Similar phenomena can be observed when rectangular specimens with the holes along the transverse direction are stretched (Figure 4d and e). It is worth mentioning that the deformed holes located up and down from the central hole exhibit C_2 symmetry but have a mirror plane along the machinery direction rather than the transverse direction, and that the central holes are not deformed as much as those of the rectangular specimen with holes along the machinery direction, which should be related with the results of tensile forces represented in Figure 3b. In order to study the

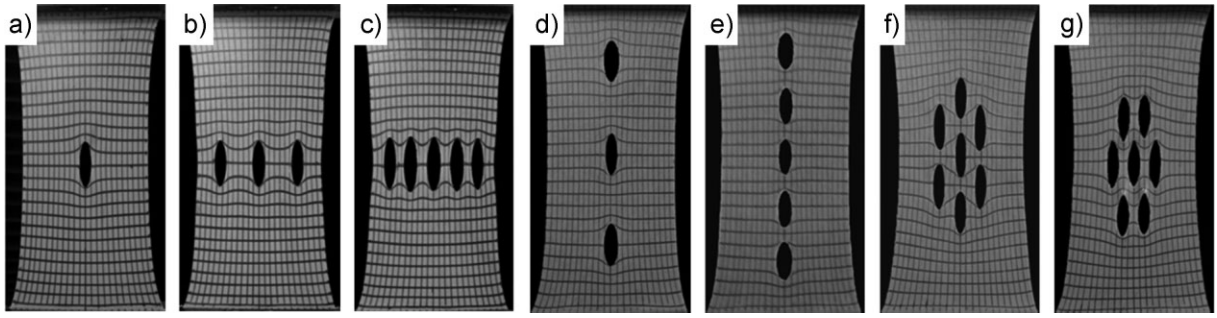

Figure 4. Photographs of rectangular specimen at 80% elongation: (a) with one hole at the center, (b, d) with three holes, (c, e) with five holes, and (f, g) with seven holes. Figure 5b and d have three holes on the transverse direction (*x*-axis) of HSPS with 0° polar angle (Figure 1j) and on the machinery direction (*y*-axis) of HSPS with 30° polar angle (Figure 1k), respectively. Figure 5c and e have five holes on the transverse direction (*x*-axis) of HSPS with 30° polar angle (Figure 1k) and on the machinery direction (*y*-axis) of HSPS with 0° polar angle (Figure 1j), respectively. Figure 5f and g are HSPS with seven holes corresponding to Figure 1j and k, respectively.

cooperative contributions of stress concentrations, seven holes are first punched in the honeycomb structure on the rectangular specimen and they are stretched up to 80% elongation along the 0 and 30° polar angles, as shown in Figure 4f and g, respectively. As shown in Figure 4a–e, the shapes of the stretched holes are different compared with those of the central ones, even though their symmetry is C_{2v}. This result indicates that the stress around the central hole is affected by the neighboring holes located not only on the *x*- and *y*-axes but also on the quadrant planes. It is also recognized that the stress concentrations around the central holes decrease as increasing the number of holes and this decrease is more effective when the holes are arranged along the machinery direction (Figure 4). The deformed square meshes drawn on the in-plane (*xy*-plane) surface of the rectangular samples clearly demonstrate the stress distributions at the 80% elongation, as shown in Figure 4a–g.

Tensile Properties of HSPS as a Function of Polar Angle

To investigate the cooperative contribution of the stress concentration and to construct the structure/property relationships of the patterned polymer architecture depending on the symmetry, the rectangular specimens with seven holes punched in the honeycomb structure are first studied, as shown in Figure 4f and g. However, the rectangular specimens with seven holes at the first round honeycomb structure are fairly limited to extract the data for this study so that the rectangular specimens with 19 holes up to the second round honeycomb structure are prepared and mechanically deformed. Figure 5a and b represent the tensile forces and their corresponding in-plane surface areas of NBR HSPS with 19 holes at 80% elongation as a function of the polar angle. Figure 5a clearly demonstrates that upon varying the polar angle from 0 to 30°, the tensile forces fluctuate up and down like an undamped negative sinusoidal wave with a wavelength of 15° in the polar angle. This result should come from the combined reasons, such as symmetry, edge effect, and

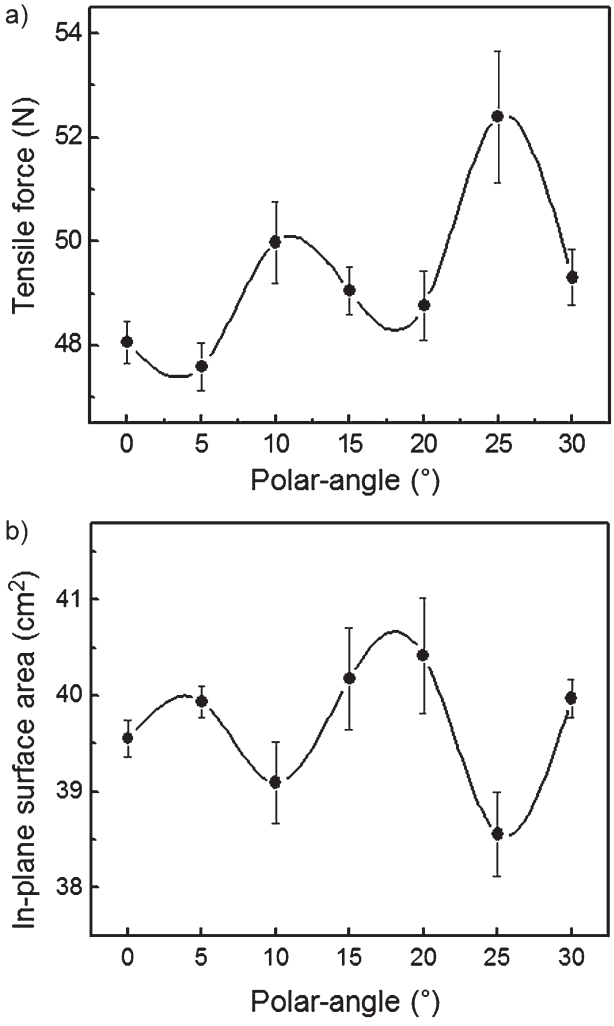

Figure 5. (a) Tensile forces and (b) their corresponding in-plane surface areas of NBR HSPS with 19 holes at 80% elongation as a function of the polar angle from 0 to 30°.

stress concentration. In the aspect of symmetry, this result can be explained by the fact that the symmetric HSPS structure (polar angle = 0 and 30°) can be elongated with a lower tensile force compared with the asymmetric one

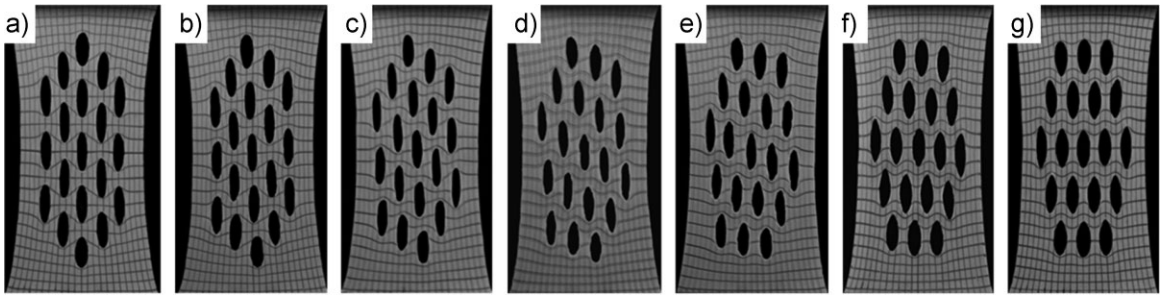

Figure 6. Photographs of NBR HSPS with 19 holes at 80% elongation by changing polar angles: (a) 0, (b) 5, (c) 10, (d) 15, (e) 20, (f) 25, and (g) 30°.

(polar angle = 10 and 25°). Furthermore, it is also realized that the holes aligned along the machinery direction is more effective to decrease the tensile force at 80% elongation than the holes located along the transverse direction, which is well matched with the results extracted from Figure 3 and 4. In Figure 5a, the tensile force is used rather than the tensile stress because the cross-section area of HSPS with respect to the polar angle is continually changed during the tensile test. However, the tensile forces according to the different polar angles could be related with the in-plane surface areas which can be easily monitored during the tensile tests. Here, the in-plane surface area at the 80% elongation is measured by considering the NBR part. Similar to the tensile forces, the in-plane surface area of the deformed HSPS at the 80% elongation also undulates with the 15° wavelength of polar angle, but like an undamped positive sinusoidal wave. This result confirms that the holes stretched along the asymmetric axis (polar angle = 10 and 25°) are deformed more than those stretched along the symmetric axis (polar angle = 0 and 30°). Based on the simple tensile test of HSPS with respect to the polar angle, it can be concluded that the holes aligned along the apex of honeycomb structure in HSPS are more effective to decrease the tensile force than those located along the plane of honeycomb structure.

Upon stretching HSPS along the different polar angles from 0 to 30°, the stress concentration and distribution of HSPS with 19 holes are also monitored and their photographs at the 80% elongation are represented in Figure 6a–g, respectively. The deformed square meshes, exhibiting the local deformations and stress concentrations, are surprisingly well matched with the computer-simulated results for the deformed hexagonal structure of diblock copolymers in the nanometer length scale.[42–44] This result means that, even though this research looking for the correlation between the mechanical property and the deformed morphology of the patterned polymer structure cannot provide quantitative values in the different length scale, this research can provide the intuitive experimental pictures for the construction of the structure/property relationships of the patterned polymer architecture depending on the symmetry. As expected, the central holes in the symmetrically stretched HSPS (polar angle = 0 and 30°) retain the C_{2v} symmetry, while other holes including the central holes in the asymmetrically stretched HSPS (polar angle = 5, 10, 15, 20, and 25°) lose the mirror and rotational symmetries. It is worth noting that the deformed five holes on the transverse direction at the polar angle = 30° shown in Figure 6g are quite different from those represented in Figure 4c. The central hole in Figure 4c is elongated most while the stress in Figure 6g is concentrated most on the side edge of the holes which are located at the edge in HSPS. This difference should come from the holes out of the transverse direction, which delocalizes the stress concentration at the center. This explanation is also supported by the observation that the stress is concentrated most on the holes having the least number of neighboring holes, as shown in Figure 6a–g. Therefore, it is realized that the introduction of defects around the stress concentrated position is quite effective in releasing the stress.

NBR molecules at the highly stretched regions should be aligned along the machinery direction and show the anisotropic birefringence. Anisotropic molecular arrangements can be evaluated by the structure-sensitive scattering techniques and polarized optical microscopy. However, NBR HSPS are too thick to obtain X-ray scattering patterns, and optical microscopy is not suitable for NBR. Therefore, in order to monitor molecular orientations in HSPS, PDMS HSPS samples are prepared as the identical geometry of NBR HSPS and deformed between the cross-polarized films. Figure 7a–g represent the photographs of PDMS HSPS with 19 holes at 20% elongation while changing the polar angle from 0 to 30°. In general, when PDMS molecules are aligned parallel to the machinery direction (*y*-axis, the polarizer direction), to the transverse direction (*x*-axis, the analyzer direction) or to the HSPS normal direction (*z*-axis, the light propagation direction), the bright state can be obtained on the photographs of the stretched PDMS HSPS, as shown in Figure 7a–g. Among three possibilities, the molecular orientation along the machinery direction (*y*-axis, the stretched direction) is the most probable situation to show birefringence in this system. In Figure 7a–g, the degree of PDMS molecular orientation depending on the different

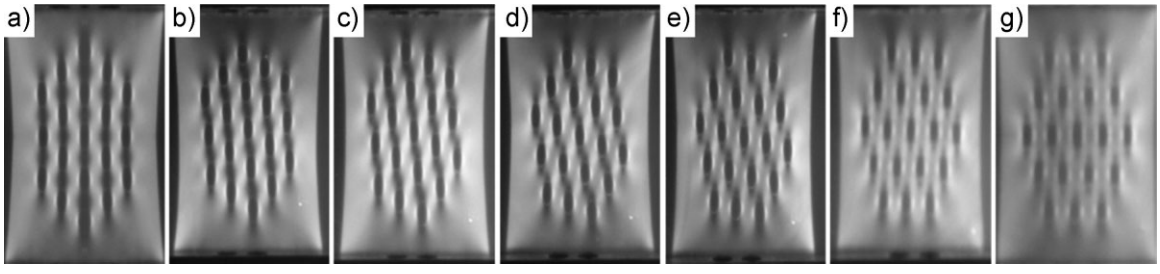

Figure 7. Photographs of PDMS HSPS with 19 holes at 20% elongation by changing polar angles: (a) 0, (b) 5, (c) 10, (d) 15, (e) 20, (f) 25, and (g) 30°.

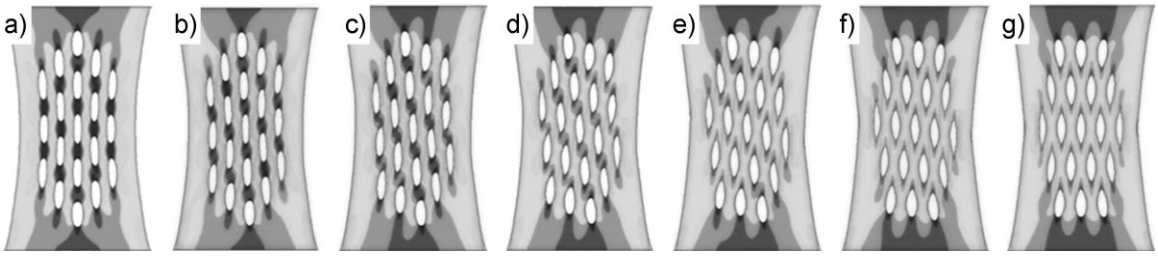

Figure 8. FEA computer simulated HSPS images at 80% elongation: (a) 0, (b) 5, (c) 10, (d) 15, (e) 20, (f) 25, and (g) 30°.

location is shown as the intensity of penetrated light. The distribution of penetrated light and its intensity (Figure 6a–g) are well matched with the results obtained from NBR HSPS (Figure 7a–g). From this result, it can be concluded that NBR molecules are anisotropically oriented along the stretched direction at the stress concentrated region.

Computer-simulated HSPS images at the 80% elongation are also obtained by using FEA techniques and their results with respect to the polar angle from 0 to 30° are shown in Figure 8a–g. Again, the calculated stress distributions and the deformed HSPS morphologies (Figure 8a–g) agree well with the experimental data (Figure 6a–g).

Conclusion

Mechanical properties of 2D HSPS are studies with respect to the polar angle of the honeycomb structure in order to construct the structure/property relationships of the patterned polymer architecture depending on the symmetry. The holes aligned along the apex of honeycomb structure are more effective to decrease the tensile force than those located along the plane. Upon varying the polar angle from 0 to 30°, the tensile force fluctuates up and down like an undamped negative sinusoidal wave with a wavelength of 15° in the polar angle. The in-plane surface area of the deformed HSPS at 80% elongation also undulates with a wavelength of 15° in the polar angle, but like an undamped positive sinusoidal wave. Stress concentrations as stretching HSPS along the polar angle from 0 to 30° are also monitored by the deformed meshes drawn on the in-plane surface, which results are well matched with those of FEA computer simulation. Furthermore, the polymer molecular orientations at specific locations of HSPS are investigated by the in situ change of birefringence under cross-polarized films. It is also recognized that the stress concentration around the central hole decreases with the number of holes and this decrease is more effective when the holes are arranged along the machinery direction. Based on experimental results combined with computer simulations, it is concluded that the tensile force of HSPS does depend on the number of holes as well as the symmetry of the honeycomb structure. This results can give insight information for tunable smart materials which can be applied in the fields of the optoelectronic devices and biochemical sensors.

Acknowledgements: This work was supported by the *National Space Lab program* (S1 08A01003210) and the *World Class University program* (R33-2008-000-10016-0) from the *Ministry of Knowledge Economy, Korea*. K.-U. J. would like to acknowledge the 2007 *New Faculty Supporting Program* of *Chonbuk National University* (1063770100).

Received: November 15, 2010; Revised: December 27, 2010; Published online: February 21, 2011; DOI: 10.1002/macp.201000708

Keywords: honeycomb structure; large deformations; morphology; stress; symmetry

[1] Q.-Z. Fang, T. J. Wang, H.-M. Li, *Polymer* **2006**, *47*, 5174.
[2] S. Singamaneni, K. Bertoldi, S. Chang, J.-H. Jang, S. L. Young, E. L. Thomas, M. C. Boyce, V. V. Tsukruk, *Adv. Funct. Mater.* **2009**, *19*, 1426.
[3] N. T. Qazvini, N. Mohammadi, *Polymer* **2005**, *46*, 9088.
[4] W. Ren, P. J. McMullan, A. C. Griffin, *Macromol. Chem. Phys.* **2008**, *209*, 1896.
[5] P. Jiang, J. F. Bertone, K. S. Hwang, V. L. Colvin, *Chem. Mater.* **1999**, *11*, 2132.
[6] Y. Xu, B. Zhu, Y. Xu, *Polymer* **2005**, *46*, 713.
[7] J.-S. Yu, S. Kang, S. B. Yoon, G. Chai, *J. Am. Chem. Soc.* **2002**, *124*, 9382.
[8] L. Li, Y. Zhong, C. Ma, J. Li, C. Chen, A. Zhang, D. Tang, S. Xie, Z. Ma, *Chem. Mater.* **2009**, *21*, 4977.
[9] N. Maruyama, T. Koito, J. Nishida, T. Sawadaishi, X. Cieren, K. Ijiro, O. Karthaus, M. Shimomura, *Thin Solid Films* **1998**, *327*, 854.
[10] H. Míguez, S. M. Yang, N. Tétreault, G. A. Ozin, *Adv. Mater.* **2002**, *14*, 1805.
[11] S. H. Park, Y. Xia, *Adv. Mater.* **1998**, *10*, 1045.
[12] B. de Boer, U. Stalmach, H. Nijland, G. Hadziioannou, *Adv. Mater.* **2000**, *12*, 1581.
[13] C. X. Cheng, Y. Tian, Y. Q. Shi, R. P. Tang, F. Xi, *Langmuir* **2005**, *21*, 6576.
[14] A. Imhof, D. J. Pine, *Nature* **1997**, *389*, 948.
[15] Y. Tian, H. Ding, Q. Jiao, Y. Shi, *Macromol. Chem. Phys.* **2006**, *207*, 545.
[16] Y. Tian, S. Liu, H. Ding, L. Wang, B. Liu, Y. Shi, *Macromol. Chem. Phys.* **2006**, *207*, 1998.
[17] J.-H. Jang, C. K. Ullal, T. Choi, M. C. LeMieux, V. V. Tsukruk, E. L. Thomas, *Adv. Mater.* **2006**, *29*, 2123.

[18] S. Z. D. Cheng, *J. Polym. Sci., Part B: Polym. Phys.* **2005**, *43*, 3361.
[19] S. Jinxia, L. Heng, H. Pingsheng, *Chin. Sci. Bull.* **2004**, *49*, 1431.
[20] J. M. Lehn, *Proc. Natl. Acad. Sci. USA* **2002**, *99*, 4763.
[21] K.-U. Jeong, S. Jin, J. J. Ge, B. S. Knapp, M. J. Graham, J. Ruan, M. Guo, H. Xiong, F. W. Harris, S. Z. D. Cheng, *Chem. Mater.* **2005**, *17*, 2852.
[22] M. Mamodia, K. Indukuri, E. T. Atkins, W. H. Jeu, A. J. Lesser, *J. Mater. Sci.* **2008**, *43*, 7035.
[23] D. Pavlović, J. G. Linhardt, J. F. Künzler, D. A. Shipp, *Macromol. Chem. Phys.* **2010**, *211*, 1482.
[24] U. H. F. Bunz, *Adv. Mater.* **2006**, *18*, 973.
[25] T. Choi, J. H. Jang, C. K. Ullal, M. C. LeMieux, V. V. Tsukruk, E. L. Thomas, *Adv. Fucnt. Mater.* **2006**, *16*, 1324.
[26] C. Park, J. Yoon, E. L. Thomas, *Polymer* **2003**, *44*, 6725.
[27] C. Yu, J. Zhai, X. Gao, M. Wan, L. Jiang, T. Li, Z. Li, *J. Phys. Chem. B* **2004**, *108*, 4586.
[28] S. J. Park, S. H. Hwang, N. Kim, S. W. Kuo, H. Y. Kim, Y. J. Kim, C. Nah, J. H. Lee, K.-U. Jeong, *J. Phys. Chem. B* **2009**, *113*, 13499.
[29] M. A. Villar, D. R. Rueda, F. Ania, E. L. Thomas, *Polymer* **2002**, *43*, 5139.
[30] H. N. Lee, R. A. Riggleman, J. J. Pablo, M. D. Ediger, *Macromolecules* **2009**, *42*, 4328.
[31] S. Han, A. L. Briseno, X. Shi, D. A. Mah, F. Zhou, *J. Phys. Chem. B* **2002**, *106*, 6465.
[32] M. E. Fares, M. K. Elmarghany, *Comp. Struct.* **2008**, *82*, 71.
[33] C. C. Honeker, E. L. Thomas, R. J. Albalak, D. A. Hajduk, S. M. Gruner, M. C. Capel, *Macromolecules* **2000**, *33*, 9395.
[34] C. C. Honeker, E. L. Thomas, *Macromolecules* **2000**, *33*, 9407.
[35] N. Artzi, M. Narkis, A. Siegmann, *J. Polym. Sci., Part B: Polym. Phys.* **2005**, *43*, 1931.
[36] M. Srinivasarao, D. Collings, A. Philips, S. Patel, *Science* **2001**, *292*, 79.
[37] H. Yabu, R. Jia, Y. Matsuo, K. Ijiro, S. Yamamoto, F. Nishino, T. Takaki, M. Kuwahara, M. Shimomura, *Adv. Mater.* **2008**, *20*, 4200.
[38] C. H. Park, S. G. Louie, *Nano Lett.* **2008**, *8*, 2200.
[39] C. Nah, J. M. Rhee, C. H. Yoon, Y. I. Huh, S.-C. Han, *Elastomer* **2000**, *35*, 173.
[40] B. Meissner, L. Matejka, *Polymer* **2001**, *42*, 1143.
[41] B. Meissner, L. Matejka, *Polymer* **2008**, *49*, 2560.
[42] J. Zhang, S. Hu, J. Rieger, S. V. Roth, R. Gehrke, Y. Men, *Macromolecules* **2009**, *42*, 4795.
[43] T. Nishikawa, M. Nonomura, K. Arai, J. Hayashi, T. Sawadaishi, Y. Nishiura, M. Hara, M. Shimomura, *Langmuir* **2003**, *19*, 6193.
[44] Z. C. Lin, J. C. Huang, *J. Mater. Process Technol.* **2008**, *201*, 477.